The origin of the *Gaia* phase-plane spiral

James Binney[⋆] and Ralph Schönrich

Rudolf Peierls Centre for Theoretical Physics, Clarendon Laboratory, Oxford OX1 3PU, UK

ABSTRACT

A simple model is presented of the formation of the spiral in the (z, v_z) phase plane of solar-neighbourhood stars that was recently discovered in *Gaia* data. The key is that the frequency Ω_z at which stars oscillate vertically depends on angular momentum about the z-axis in addition to the amplitude of the star's vertical oscillations. Spirals should form in both $\langle v_\phi \rangle$ and $\langle v_R \rangle$ whenever a massive substructure, such as the Sgr dwarf galaxy, passes through the Galactic plane. The model yields similar spirals to those observed in both $\langle v_\phi \rangle$ and $\langle v_R \rangle$. The primary driver is the component of the tidal force that lies in the plane. We investigate the longevity of the spirals and the mass of the substructure, but the approximations inherent in the model make quantitative results unreliable. The work relies heavily on a self-consistent, multicomponent model of our Galaxy produced by the AGAMA package for $f(\boldsymbol{J})$ modelling.

Key words: methods: numerical – Galaxy: kinematics and dynamics – galaxies: kinematics and dynamics.

1 INTRODUCTION

The second data release from the *Gaia* mission (DR2; Gaia Collaboration 2018) revealed an unexpected spiral pattern in the phase plane (z, v_z) associated with oscillations perpendicular to the Galactic plane of stars that lie in a thin cylindrical shell around the Sun and are located at similar Galactocentric azimuthal coordinates to that of the Sun (Antoja et al. 2018). The spiral is barely visible in a plot of the density ρ of stars in the (z, v_z) plane but clearly visible in a plot in this plane of $\langle v_\phi \rangle$, the mean value of the component of velocity in the direction of Galactic rotation. As Antoja et al. (2018) remark, this feature is suggestive of the phase-winding of a group of stars that start strongly clumped in the (z, v_z) plane because such a clump would shear into a spiral of the observed handedness as a consequence of the vertical period of oscillation being an increasing function of their amplitudes – the vertical oscillations of stars are strongly anharmonic.

While we shall see that this intuition is sound, it does not explain why the spiral is so much more clearly visible in $\langle v_\phi \rangle(z, v_z)$ than in $\rho(z, v_z)$, nor does it explain the origin of the putative clump.

Here, we use the technique of $f(\boldsymbol{J})$ modelling (Binney 2010; Piffl, Penoyre & Binney 2015; Pascale et al. 2018) to show how an 'intruder', such as a dwarf galaxy or a pure dark-matter structure, that passes through the disc near the pericentre of its orbit generates a feature like that observed.

In Section 2, we outline both the model Galaxy and the data from *Gaia* DR2 on which we rely. Section 3 contains the paper's core: a qualitative explanation of how a passing massive body perturbs

the disc leads in Section 3.1 to a simple quantitative model that can produce a spiral like that observed. Then in Section 3.2 we explain how the spiral emerges and in Section 3.3 we investigate its longevity. In Section 3.4, we show that a similar but distinct spiral is expected in v_R, and we display this spiral in both the model and *Gaia* data. Section 4 discusses the model's strengths and weaknesses, concluding that full *N*-body simulation is needed. Section 5 sums up and looks to the future.

2 UNDERPINNINGS

2.1 The underlying Galaxy model

Our work involves perturbing a model Galaxy that has been fitted to the subsample of Gaia DR2 that comprises stars with measured line-of-sight velocities (Soubiran et al. 2018). These stars are so numerous and cover such a significant range of radii that their kinematics when binned in ranges of R and z suffice to constrain strongly the structure of the Galaxy's discs, stellar halo and dark halo (Binney & Vasiliev in preparation). The model is defined by distribution functions $f(\boldsymbol{J})$ that are analytic functions of the action integrals $\boldsymbol{J} = (J_r, J_z, J_\phi)$. The bulge, the stellar halo, the low-α disc, the high-α disc, and the dark halo are all assigned an $f(\boldsymbol{J})$ and the parameters within the $f(\boldsymbol{J})$ are adjusted until the predicted stellar kinematics provide reasonable fits to the DR2 data. After each change of the parameters, the software package AGAMA (Vasiliev 2018) is used to solve for the potential that the bulge, discs, and dark halo jointly generate alongside a fixed representation of the mass of the interstellar medium. Hence, the final (axisymmetric) model is fully self-consistent, and strongly constrained within the radial range covered by the DR2 data. It very nicely reproduces the

⋆ E-mail: binney@thphys.ox.ac.uk

vertical density profile that Gilmore & Reid (1983) used to discover the thick disc (now better termed the high-α disc).

2.2 Data from *Gaia* DR2

We use the radial velocity subset of *Gaia* DR2 (Soubiran et al. 2018), which comprises more than 7 million stars with full 6D phase-space information, i.e. positions, parallaxes, proper motions, and line-of-sight velocity measurements. Heliocentric stellar positions and velocities are translated into the Galactic frame assuming the Sun's Galactocentric radius and vertical position are $(R_0, z_0) = (8.27, 0.02)$ kpc (Joshi 2007; Schönrich, Binney & Dehnen 2010; Schönrich 2012), and its Galactocentric motion is $(U_0, V_0, W_0) = (11.1, 250, 7.24)$ km s^{-1}, so the Sun is moving inwards and upwards.

We assign distances to stars using the iterative method of Schönrich & Aumer (2017), which has been validated on *Gaia* DR1 (Lindegren et al. 2016) matched with the RAVE (Kunder et al. 2017) and LAMOST surveys. By using a self-generated prior on distance, this method ensures unbiased distances for every sample, and statistically validates the distances.

The *Gaia* DR2 parallaxes have significant zero-point errors (Lindegren et al. 2018). For the sake of simplicity, we here add $\delta\varpi = 0.048$ mas to all published parallaxes (Schönrich et al. in preparation). We use only stars that (i) satisfy the parallax quality cut $\sigma_\varpi/\varpi < 0.2$, (ii) have ≥ 5 visibility periods, and (iii) have 'excess noise' < 1 mas. In the plots below, we use stars that lie in the region $|R - R_0| < 0.5$ kpc, $|y| < 4$ kpc, $|z| < 1.5$ kpc.

3 THE PHYSICS OF THE PHASE-PLANE SPIRAL

From the fact that the spiral appears clearly in a plot of $\langle v_\phi \rangle$ in a narrow range of R it follows that it is associated with a correlation between the in-plane oscillations (radial epicyclic motion) and oscillations perpendicular to the plane. The passage of an intruder through the plane will inevitably generate such correlated oscillations. Indeed, consider an intruder that passes vertically down through the plane such that its velocity at $z = 0$ is in the $-e_z$ direction. Throughout its passage the intruder attracts stars towards it with the consequence that the v_R and v_ϕ components of each star's velocity change steadily during the passage. The v_z component, by contrast is incremented as the intruder approaches from above, but then decremented as the intruder recedes below the plane. The decrement would cancel the increment perfectly if the star in question were stationary during the passage, but on account of the star's motion they do not quite cancel, and the star receives a net kick, which is on average downwards.

We decompose the motion of each star into two parts. The first part is the star's unperturbed motion, being part circulation and part radial and vertical oscillation. Averaged over all stars this unperturbed motion brings stars neither closer to the intruder nor further from it during the passage, so this motion does not give rise to a net vertical impulse on the Galaxy by the intruder. On the other hand, stars initially at 2 o'clock in Fig. 1, which are being carried towards the intruder by Galactic rotation, will be closer to the intruder as it recedes than they were as it approached. Hence, these stars will receive a net downward impulse. Conversely, stars initially at 4 o'clock will receive a net upward impulse. From this discussion it follows that the vertical impulse arising from rotation will be an odd function of $\phi - \phi_{\text{intruder}}$ with ϕ defined as in Fig. 1 to ensure that Galactic rotation corresponds to $\dot\phi > 0$. Rotation will most strongly
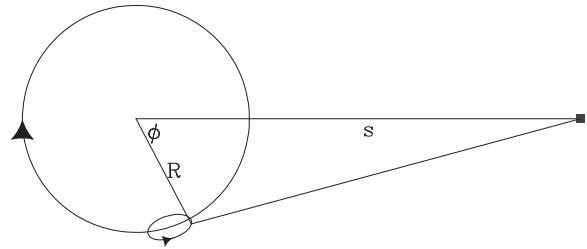

Figure 1. Schematic of the impact on a star of an intruder passing through the plane distance *s* from the GC.

impel stars downwards at $\phi - \phi_{\text{intruder}} \sim -\pi/2$, where stars are moving almost directly towards the perturber, and will impel stars most strongly upward at $\phi - \phi_{\text{intruder}} \sim \pi/2$ and have little effect when this angle is 0 or π because then it will not be changing the distance to the intruder. Given this pattern of up and down impulses, we take the contribution from rotation to the downward impulse to be $-\beta \sin(\phi - \phi_{\text{intruder}})$ times the in-plane impulse.

The second part of the motion of stars is the motion arising from the pull of the intruder. On average this moves stars towards the intruder, and thus causes the downward pull as the intruder recedes to exceed the upward pull as the intruder approaches. Hence, the pull of the intruder towards its line of flight always generates a net downward kick. This is essentially the physics of dynamical friction.

3.1 A toy model

With AGAMA one can quickly sample the stellar DF subject to any selection function $g(\mathbf{x})$. We used this facility to choose phase-space coordinates for a million stars that lie within the region

$$R_0 - 0.5 \text{ kpc} < R < R_0 + 0.5 \text{ kpc} \qquad |\phi - \phi_\odot| < 0.25 \text{ rad}, \quad (1)$$

and are biased towards shorter distances in the way characteristic of the radial velocity subset of *Gaia* DR2. The orbits of these stars were then integrated backwards for a time τ. Then we computed the difference between the gravitational acceleration towards an intruder at the location $(R, z = 0, \phi = \phi_{\text{intruder}})$ on (i) a star located at $\mathbf{x}(-\tau)$ and (ii) a star located at the Galactic centre $(R = 0, z = 0)$. By subtracting the latter acceleration from the pull of the intruder, we take cognisance that we are working in the non-inertial frame in which the Galactic centre remains stationary. The kicks stars experience are proportional to the product $M \times T$ of the intruder's mass and the effective duration of the passage

$$T = \frac{2p}{v_{\text{intruder}}}, \qquad (2)$$

where $p = 10$ kpc is the impact parameter from the perspective of the solar neighbourhood and $v_{\text{intruder}} \simeq 300$ km s^{-1} is the intruder's speed. $M = 2 \times 10^{10} \text{ M}_\odot$ and $T = 66$ Myr were adopted for the figures.

Fig. 2 shows in black the current locations of 30 stars from the solar-neighbourhood sample. The red arrows are centred on the locations of these stars $\tau = 200$ Myr in the past as the intruder (blue square) passed through the plane. The lengths of the arrows are proportional to the kicks $\delta\mathbf{v}$ that these stars had just received from the intruder after allowing for the fact that the reference frame has been kicked as if it were a particle at the Galactic centre.

The acceleration computed above multiplied by a characteristic time-scale of the passage yields a velocity change $\delta\mathbf{v}_\parallel$ that lies within the plane. To this we must add a (downward) component $\delta v_\perp$ that
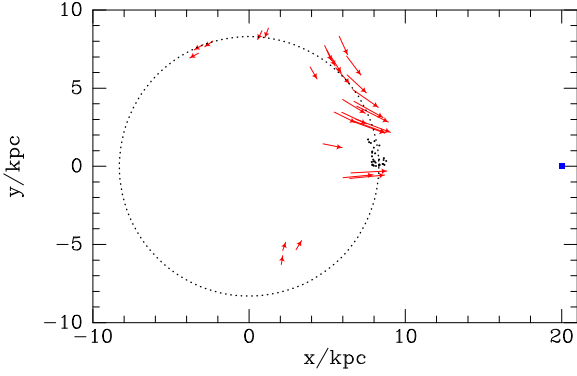
Figure 2. The centres of red arrows mark the locations 200 Myr ago of stars that are currently close to the Sun (black dots). The arrows are proportional to the tidal impulses the stars receive during the passage of the intruder, which we see crossing the plane 200 Myr ago (blue square). The solar circle is traced by the dotted black line.

arises because stars move during the encounter. As explained at the head of this section, the Fourier expansion of this velocity change in the azimuths of stars will be dominated by a constant term associated with standard dynamical friction and a term proportional to $\sin(\phi - \phi_{\text{intruder}})$. The magnitude of both terms will scale with the modulus of the in-plane component. Pending a more elaborate treatment, we adopt

$$\delta v_\perp = \alpha\, \delta v_\parallel |\,[1 - \beta \sin(\phi - \phi_{\text{intruder}})]. \qquad (3)$$

When $\beta > 0$ the downward kick is larger for stars that are initially moving towards the intruder. Below we show results for $(\alpha, \beta) = (0.4, 0.5)$. Smaller values of α and larger values of β yield less interesting figures. Setting $\beta = 0$ actually improves the clarity of the figures.

In summary, except when estimating the vertical kick $\delta v_\perp$, we imagine that the intruder's gravitational field is a Dirac delta-function in time with a magnitude that is proportional to the intruder's mass times the approximate duration of the passage in the real world. Thus, we are essentially working in the impulse approximation (Binney & Tremaine 1987, section 7.2.1).

From the velocity $v(-\tau)$ of each star that we have computed by backwards integration we subtract δv computed as above to obtain the star's velocity before the intruder appeared. At the phase-space location $[x(-\tau), v(-\tau) - \delta v]$, we evaluate the stellar DF $f(J)$ (the sum of the DFs of bulge, stellar halo, and discs) by using the Stäckel Fudge (Binney 2012) to evaluate the actions. By Liouville's theorem, this value,

$$f_0 = f[J(x, v - \delta v)], \qquad (4)$$

is the actual phase-space density at the current location of the star near the Sun. By contrast, we sampled the solar neighbourhood using the sampling density

$$f_s = f[J(x, v)], \qquad (5)$$

where J comprises the actions reached after the kick, which are conserved along the orbit from that time to the present. By the principle of Monte Carlo integration, a valid estimate of the current expectation value of any phase-space variable q is the sum over stars

$$\langle q \rangle = \frac{1}{N} \sum_{i=1}^{N} q_i \frac{f_{0i}}{f_{si}}. \qquad (6)$$
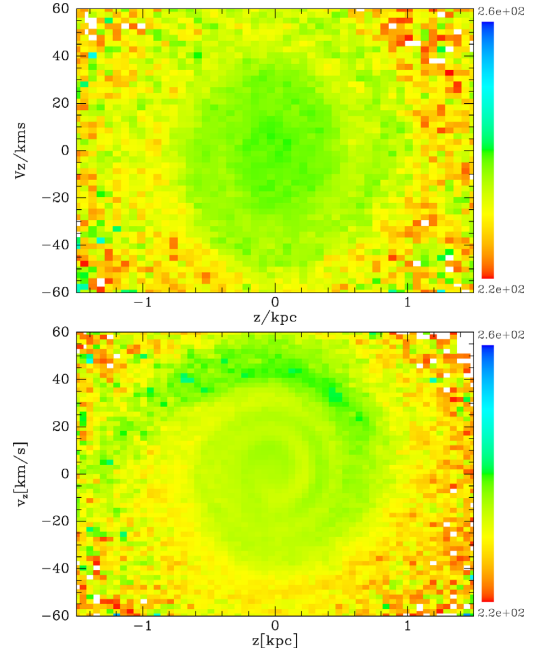

Figure 3. Upper panel: the average value of v_ϕ within the (z, v_z) phase plane computed for an impulsive passage of an intruder 400 Myr ago at a Galactocentric distance of 20 kpc. Lower panel: the same average for stars in *Gaia* DR2.
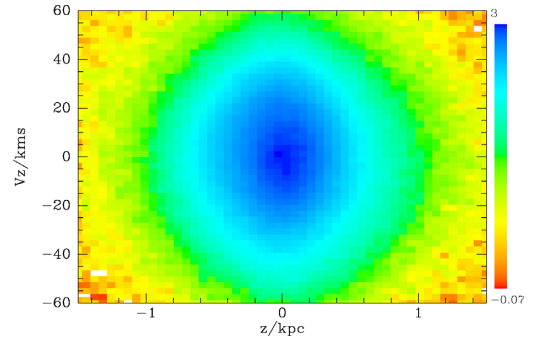

Figure 4. Density of model stars in the (z, v_z) plane.

The result of applying this formula to $q = v_\phi$ for $\alpha = 0.4$, $\beta = 0.5$, $\tau = 400$ Myr is shown in the upper panel of Fig. 3. A spiral is evident that is remarkably similar to that seen in the lower panel, which after Antoja et al. (2018) shows $\langle v_\phi \rangle$ in the *Gaia* DR2 data.

Fig. 4 shows the current density of model stars in the (z, v_z) plane: no spiral is evident just as in the corresponding plot in Antoja et al. (2018).

3.2 Moving around your ellipse

To obtain a better understanding of how the phase-plane spiral forms, the upper panel of Fig. 5 shows the distribution of stars in the plane $(\sqrt{J_z}, \Omega_z)$. $\sqrt{J_z}$ is the natural radial coordinate in the (z, v_z) plane: in this plane stars move clockwise on ellipses of area $2\pi J_z$. Stars lie in a broad swath that extends from large Ω_z at small J_z to small Ω_z at large J_z, and it was to this trend of Ω_z with J_z that Antoja et al. (2018) appealed in their picture of phase-wrapping of a clump of stars. As remarked in the Section 1, the problem with this explanation is the invisibility of a spiral in the density $\rho(z, v_z)$.
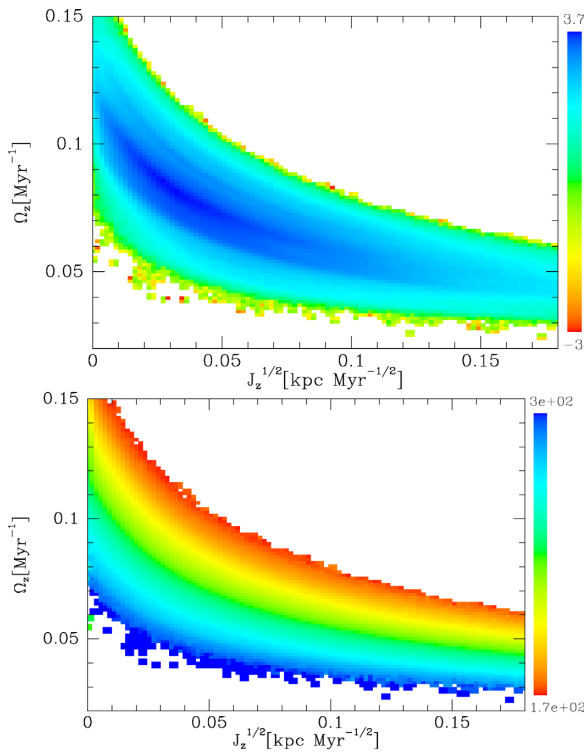
Figure 5. Upper panel: from *Gaia* DR2 we show the density of stars in the plane ($J_z^{1/2}$, Ω_z). Lower panel: the mean value of v_ϕ within this plane.
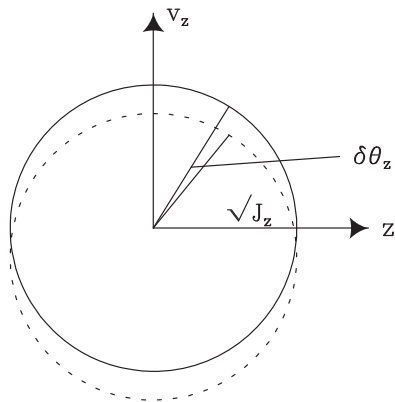

Figure 6. Schematic of the (z, v_z) plane showing the effect on the DF of decrementing all values of v_z. Initially the full ellipse, a curve of constant J_z, is a contour of f. After velocities have been decremented, this contour becomes the dashed curve, which is not a curve of constant J_z. Consequently, on curves of constant J_z stars are concentrated towards $\theta_z = \pi$ since the origin of θ_z is conventionally at the top of the curves.

The lower panel of Fig. 5 reveals the reason for the width of the swath by plotting $\langle v_\phi \rangle$, the average value of v_ϕ in each pixel. This forms a perfect rainbow, with low $\langle v_\phi \rangle$ at the top of the swath and high $\langle v_\phi \rangle$ at the bottom. This correlation arises because all stellar frequencies decrease as one moves out through the Galaxy, and in the solar neighbourhood v_ϕ is tightly connected to J_ϕ, which controls an orbit's guiding-centre radius.

By Jeans theorem, in a relaxed Galaxy the distribution of stars is stratified in the (z, v_z) plane on ellipses of constant J_z, so it is independent of θ_z. The intruder shifts the distribution of stars down in the (z, v_z) plane so it is no longer stratified by J_z (Fig. 6).
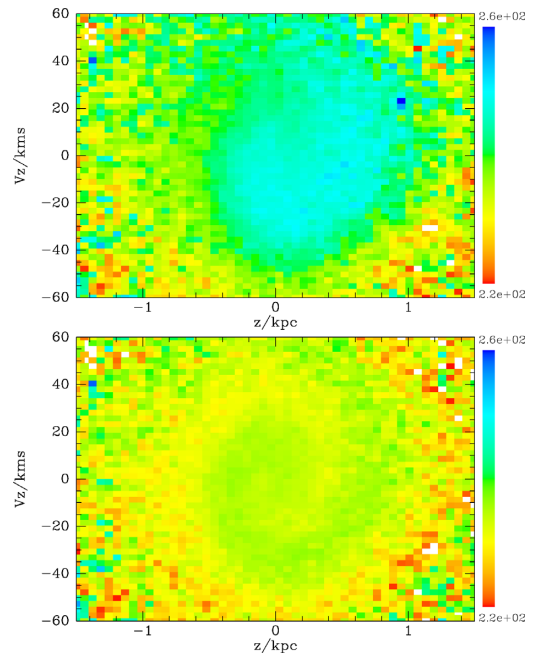

Figure 7. Upper panel: $\langle v_\phi \rangle$ 100 Myr after a passage. Lower panel: $\langle v_\phi \rangle$ 200 Myr after a passage.

Hence, the distribution is now a function of the conjugate angle θ_z in addition to J_z, with a concentration of stars at $\theta_z = \pi$.[1] After the perturbation has been applied, each star moves around its newly assigned ellipse at a rate Ω_z that varies systematically with v_ϕ. Hence, in the top panel of Fig. 3 the colour of an ellipse varies with location θ_z around it. On account of the dependence of Ω_z on J_z, the colouration evolves on smaller ellipses faster than on larger ellipses. Hence, the emergence of the spiral depends essentially on both functional dependencies of $\Omega_z(J_\phi, J_r)$.

3.3 How long does a spiral last?

In Fig. 7, we show $\langle v_\phi \rangle$ in the phase plane 100 Myr (upper panel) and 200 Myr (lower panel) after an intruder passed through the plane. In each case the intruder passed through the disc at what was at that time the mean azimuth of the sampled stars. Hence, the stars that contribute to the upper panel have gone half way round the Galaxy since they were kicked, while those in the lower panel have been round once. In the upper panel the spiral is still forming, while in the lower panel it is less wound up that that seen in the data. The amplitude of the spiral does not vary much between 100 and 400 Myr, all that varies is the degree of winding. Comparison of Figs 3 and 7 with the data suggests that the spiral was created 400 ± 150 Myr ago as Antoja et al. (2018) proposed. Interestingly, this is roughly how long in the past lies the previous pericentre passage of the Sgr dwarf (e.g. Dierickx & Loeb 2017).

3.4 A spiral in v_R

The intruder pulls stars outwards and thus causes an overdensity of stars in the (R, v_R) phase plane around $\theta_R = \pi/2$ (maximum outward speed) – the phase-plane geometry is extremely similar to

---

[1] We adopt the convention of TM (Binney & McMillan 2016) that $\theta_z = 0$ as stars move up through the plane.
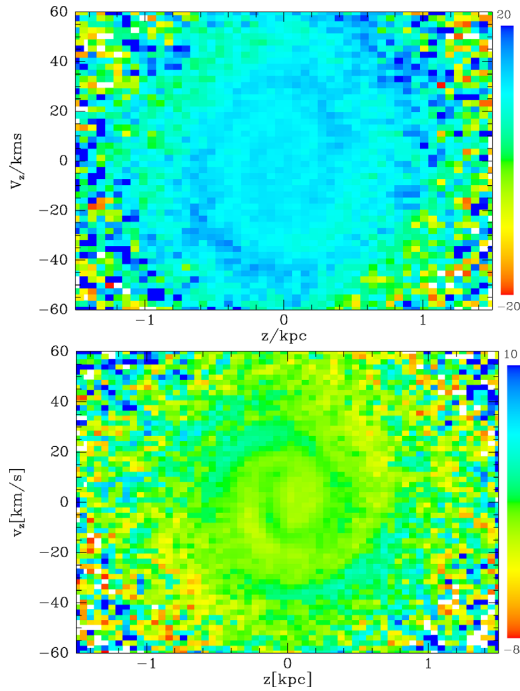
Figure 8. Upper panel: $\langle v_R \rangle$ in the phase plane at 400 Myr. Lower panel: the same mean over stars in *Gaia* DR2 that have $|v_R| < 30\,\mathrm{km\,s^{-1}}$.

that shown in Fig. 6. If at this instant we were to plot $\langle v_R \rangle$ in the (z, v_z) plane, the plot would show a coherent region of positivity rather than the uniform zero characteristic of an equilibrium disc. Now focus on the stars that lie at a point of the (z, v_z) plane where $\langle v_R \rangle > 0$. They have a common value of J_z and move around a common ellipse, but at rates Ω_z that increase as J_ϕ decreases. As J_ϕ decreases Ω_r, like Ω_z, increases, so the θ_r values of the stars that move fastest around the ellipse increase fastest. As θ_r changes, so do the v_R values of these stars, so the contribution of these stars to $\langle v_R \rangle$ changes faster than do the contributions of the groups of stars that lag them. It follows that the blob of colour signalling $\langle v_R \rangle > 0$ is sheared into a spiral that differs in the tightness of its winding from the spiral seen in $\langle v_\phi \rangle$ because v_ϕ and v_R evolve differently as θ_r increments.

The upper panel of Fig. 8 shows $\langle v_R \rangle$ in the phase plane 400 Myr after a passage. As expected, a spiral is evident that is similar to, but different from, that seen in the corresponding plot for $\langle v_\phi \rangle$. The lower panel of Fig. 8 shows a similar spiral in the *Gaia* DR2 data.

Plots of $\langle v_R \rangle$ at 100 and 200 Myr show less tightly would spirals.

4 DISCUSSION

We have supposed the action of the intruder to be impulsive in order to obtain the simplest physical picture that can explain the observed phenomenon. In reality the impulse approximation will provide only a mediocre quantitative account of the passage through pericentre of a galaxy such as Sgr. Indeed, the passage has a characteristic time-scale $T \sim 66$ Myr (equation 2) while stars near the Sun have vertical periods down to ~ 40 Myr (Fig. 5). The radial and azimuthal period are longer, but rarely long enough for the impulse approximation to be safe. The phase spiral is a phenomenon that involves several comparable time-scales so is analytically intractable. Moreover, in the limit $v_{\mathrm{intruder}} \to \infty$ in which the impulse approximation becomes exact, the phenomenon under discussion will disappear because in

this limit $\delta v_\perp/\delta v_\| \to 0$. Hence, quantitative results extracted from the model presented here should be regarded with some scepticism.

However, the major weakness of the present model is not its use of the impulse approximation, which has a history of being more successful than one has a right to expect (Alladin & Narasimhan 1982; Binney & Tremaine 1987, section 7.2.1), but in the use of unperturbed frequencies Ω_z: when a whole section of the disc is pulled down, stars will oscillate vertically with significantly longer periods than $2\pi/\Omega_z$. This principle is illustrated in extreme form by the classic study of Hunter & Toomre (1969), who considered a disc of razor-thin rings. To convert a galactic disc to a razor-thin disc we must compress it along z until the density in the plane is infinite. In this process every star's frequency Ω_z diverges. Yet Hunter & Toomre (1969) showed that material points on the spinning rings oscillate up and down at perfectly finite frequencies because their neighbours move with them. What the present model gets right is the insight that the frequencies of vertical and radial oscillations decrease as J_ϕ and thus v_ϕ increase. Qualitatively, the explanation we have given is sound even though it is quantitatively significantly off.

Careful comparison of the upper and lower panels of Figs 3 and 8 reveals quantitative weaknesses. Most obviously, the model spirals seem stretched along the velocity axis with respect to those in the *Gaia* DR2 data, implying that the model's potential is not quite right.

The mass and impact parameter of the intruder are significant issues. Uncomfortably large values of the product MT of intruder mass and passage duration were required to obtain clear model spirals. With such large values of MT stars receive significant kicks and the ratio f_0/f_s of the values taken by the unperturbed DF at a star's location before and after kicking differ considerably from unity. Comparison of the colouring in the upper and lower panels of Fig. 8 suggests that the model passages are generating larger values of v_R than they should be.

Another issue is the adopted magnitude of the applied downward kicks $\delta v_\perp$ (equation 3). As was explained at the start of Section 3, the relationship of this kick to the in-plane kick depends on the intruder's speed. We have not attempted to compute it, but simply adopted a value that generates reasonable spirals. The value we have adopted is on the large side, but smaller values do not yield good figures.

Large values of $\delta v_\perp$ imply a slow intruder, which implies pericentre of a tightly bound, low eccentricity orbit. The Sgr dwarf has just such an orbit (Dierickx & Loeb 2017). However, our impulse approximation is least justifiable in this regime: an individual passage will be slow, and the data may contain signals from more than one passage, so our picture could be seriously oversimplified. Moreover, the orbit of the Sgr dwarf cuts the disc at a significantly oblique angle rather than at right angles as in our model.

To overcome the weakness of our approach both with respect to the likely slowness and recurrence of the passages and the need to recognize that whole sections of the disc are moved up and down, full N-body modelling is required. Such models (e.g. Laporte et al. 2018; Tepper-Garcia & Bland-Hawthorn 2018) are orders of magnitude more expensive than our approach,[2] and they do not provide the same insight, but they are essential for proper exploitation of the beautiful data that are now to hand.

---

[2]The plots shown here can be computed in a few minutes on a laptop.

5 CONCLUSIONS

A simple model based on the impulse-approximation in which an intruder plucks the disc out and down produces a spiral in the (z, v_z) plane very like that discovered in $\langle v_\phi \rangle$ by Antoja et al. (2018). We have displayed from the *Gaia* DR2 data a clear spiral in $\langle v_R \rangle$ and shown that our model can reproduce this spiral also. There are indications that the intruder is not on a highly eccentric orbit, with the consequence that our use of the impulse approximation is questionable and that full *N*-body modelling will be required to explain the data satisfactorily.

Whatever the orbit of the intruder, our model necessarily neglects the fact that the intruder plucks downwards whole segments of the disc rather than individual stars from the disc, with the consequence that our model uses vertical frequencies that are systematically too high. This is a serious weakness of the model, and relegates it to 'toy' status: it captures important aspects of the problem and delivers valuable insights but oversimplifies to the point that it cannot be trusted quantitatively.

This investigation illustrates nicely an aspect of the power latent in $f(\boldsymbol{J})$ modelling. Specifically it shows the value of being able to sample our corner of the Galaxy densely: if we assume the disc has scale length $R_d = 2.5\,\mathrm{kpc}$, only 0.38 per cent of the disc's stars lie in the region we have sampled, so an *N*-body model providing the same resolution in the (z, v_z) plane would require in excess of 200 million disc stars, not counting particles needed to represent the bulge, dark halo, etc. A simulation on this scale is computationally expensive. While it is true that with current $f(\boldsymbol{J})$ software it is not possible to model correctly the collective response of the disc, so ultimately *N*-body models are essential, the software does provide the initial data for an *N*-body simulation that most closely approach an equilibrium and thus eliminate unwanted transients (Vasiliev 2018). Consequently, the way forward would seem to be speedy exploration of possibilities by $f(\boldsymbol{J})$ modelling followed by a few high-quality *N*-body simulations with initial conditions furnished by the most successful $f(\boldsymbol{J})$ models.

REFERENCES

Alladin S. M., Narasimhan K. S. V. S., 1982, Phys. Rep., 92, 339
Antoja T. et al., 2018, preprint (arXiv:e-prints)
Binney J., 2010, MNRAS, 401, 2318
Binney J., 2012, MNRAS, 426, 1324
Binney J., McMillan P. J., 2016, MNRAS, 456, 1982
Binney J., Tremaine S., 1987, Galactic Dynamics. Princeton Univ. Press, Princeton, NJ
Dierickx M. I. P., Loeb A., 2017, ApJ, 847, 42
Gaia Collaboration, 2018, preprint (arXiv:e-prints)
Gilmore G., Reid N., 1983, MNRAS, 202, 1025
Hunter C., Toomre A., 1969, ApJ, 155, 747
Joshi Y. C., 2007, MNRAS, 378, 768
Kunder A. et al., 2017, AJ, 153, 75
Laporte C. F. P., Minchev I., Johnston K. V., Gómez F. A., 2018, preprint (arXiv:e-prints)
Lindegren L. et al., 2016, A&A, 595, A4
Lindegren L. et al., 2018, A&A, 616, 2L
Pascale R., Posti L., Nipoti C., Binney J., 2018, MNRAS, 480, 927
Piffl T., Penoyre Z., Binney J., 2015, MNRAS, 451, 639
Schönrich R., 2012, MNRAS, 427, 274
Schönrich R., Aumer M., 2017, MNRAS, 472, 3979
Schönrich R., Binney J., Dehnen W., 2010, MNRAS, 403, 1829
Soubiran C., Jasniewicz G., Chemin L., Zurbach C., 2018, A&A, 616, 7
Tepper-Garcia T., Bland-Hawthorn J., 2018, MNRAS, 478, 5263
Vasiliev E., 2018, preprint (arXiv:e-prints)

This paper has been typeset from a TEX/LATEX file prepared by the author.